The EMBO Journal (2010) 29, 3646–3659 | © 2010 European Molecular Biology Organization | All Rights Reserved 0261-4189/10
www.embojournal.org

THE EMBO JOURNAL

Molecular organization and dynamics of the melatonin MT_1 receptor/RGS20/G_i protein complex reveal asymmetry of receptor dimers for RGS and G_i coupling

Pascal Maurice[1,2,9], Avais M Daulat[1,2,8,9], Rostislav Turecek[3,4], Klara Ivankova-Susankova[3], Francesco Zamponi[5], Maud Kamal[1,2], Nathalie Clement[1,2], Jean-Luc Guillaume[1,2], Bernhard Bettler[3], Céline Galès[6], Philippe Delagrange[7] and Ralf Jockers[1,2,*]

[1]Institut Cochin, Université Paris Descartes, CNRS (UMR 8104), Paris, France, [2]Inserm, Paris, France, [3]Department of Biomedicine, Institute of Physiology, University of Basel, Basel, Switzerland, [4]Institute of Experimental Medicine ASCR, Prague, Czech Republic, [5]CNRS UMR 8549, Laboratoire de Physique Théorique, Ecole Normale Supérieure, Paris, France, [6]Inserm U858-I2MR, Toulouse, France and [7]Institut de Recherches SERVIER, Suresnes, France

Functional asymmetry of G-protein-coupled receptor (GPCR) dimers has been reported for an increasing number of cases, but the molecular architecture of signalling units associated to these dimers remains unclear. Here, we characterized the molecular complex of the melatonin MT_1 receptor, which directly and constitutively couples to G_i proteins and the regulator of G-protein signalling (RGS) 20. The molecular organization of the ternary MT_1/G_i/RGS20 complex was monitored in its basal and activated state by bioluminescence resonance energy transfer between probes inserted at multiple sites of the complex. On the basis of the reported crystal structures of G_i and the RGS domain, we propose a model wherein one G_i and one RGS20 protein bind to separate protomers of MT_1 dimers in a pre-associated complex that rearranges upon agonist activation. This model was further validated with MT_1/MT_2 heterodimers. Collectively, our data extend the concept of asymmetry within GPCR dimers, reinforce the notion of receptor specificity for RGS proteins and highlight the advantage of GPCRs organized as dimers in which each protomer fulfils its specific task by binding to different GPCR-interacting proteins.

The EMBO Journal (2010) **29,** 3646–3659. doi:10.1038/emboj.2010.236; Published online 21 September 2010
Subject Categories: signal transduction; structural biology
Keywords: G protein; G-protein-coupled receptor; heterodimerization; molecular organization; RGS

*Corresponding author. INSERM U1016, CNRS (UMR 8104), Institut Cochin, Université Paris Descartes, 22 rue Méchain, Paris 75014, France. Tel.: +33 14 051 6434; Fax: +33 14 051 6430;
E-mail: ralf.jockers@inserm.fr
[8]Present address: Leslie Dan Faculty of Pharmacology, University of Toronto, Toronto, Ontario, Canada
[9]These authors contributed equally to this work

Received: 16 March 2010; accepted: 27 August 2010; published online: 21 September 2010

Introduction

Heptahelical G-protein-coupled receptors (GPCRs) represent the largest family of membrane receptors with approximately 800 members in human beings responding to a wide range of extracellular stimuli. This family of receptors controls numerous processes including neuro-transmission, cellular metabolism, inflammatory and immune responses. GPCRs are of primary therapeutic importance as they are the targets of 30–50% of currently prescribed drugs. Although GPCRs have been classically described as monomeric receptors that form a ternary complex with its ligand and heterotrimeric G protein, cumulative evidence indicates that GPCRs dimerize or oligomerize (Bouvier, 2001; George *et al*, 2002; Milligan, 2009). Despite the availability of high-resolution crystal structures for several GPCRs, little is known about the stoichiometry of receptor oligomers and receptor-associated proteins. It is now well established that monomeric GPCRs are capable of activating G proteins (Bayburt *et al*, 2007; Ernst *et al*, 2007; Whorton *et al*, 2007), implying a 1:1 stoichiometry between receptor and G protein in this minimal signalling unit. By extrapolation, one might anticipate that GPCR dimers, composed of two protomers, are binding to two G-protein units. However, no experimental evidence for such an arrangement exists. In contrast, recent research suggests that the leukotriene B4 receptor BLT1 dimer, the 5-HT_{2C} receptor and the dopamine D2 receptor dimer interact with a single G protein (Baneres *et al*, 2003; Herrick-Davis *et al*, 2005; Han *et al*, 2009). Allosteric regulation between protomers of GPCR dimers has been documented for class A and class C members (Pin *et al*, 2005; Sohy *et al*, 2007; Vilardaga *et al*, 2008; Han *et al*, 2009). The transactivation model in which the ligand binds to one protomer, whereas the second receptor protomer binds to the G protein is fully compatible with the one GPCR dimer/one G-protein stoichiometry.

A functional significance for GPCR dimerization has been proposed in several cases. This is particularly evident for the case of GPCR heterodimers in which new pharmacological entities are formed. The benefit of homodimer formation is more difficult to appreciate. A function of GPCR dimerization was proposed in receptor export to the plasma membrane (Milligan, 2010) and various, positive and negative, allosteric transactivation modes have been proposed to occur between the two protomers of the dimer (Rovira *et al*, 2010). Recently, the study of Rivero-Muller *et al* has provided compelling *in vivo* evidence for the physiological relevance of GPCR dimerization by restoring the normal luteinizing hormone (LH) actions in transgenic mice co-expressing a binding deficient and a signalling deficient form of LH receptor through functional complementation in the absence of functional wild-type receptors (Rivero-Müller *et al*, 2010).

The classical collision-based model predicting the recruitment of heterotrimeric G proteins to agonist-activated receptors followed by the rapid dissociation of the Gα and Gβγ into free subunits, was recently challenged by the observation of stable pre-associated receptor–G-protein complexes that persist during the activation process (Bunemann *et al*, 2003; Galés *et al*, 2005). Galés *et al* (2006) proposed a model wherein agonist binding induces conformational rearrangements of a pre-existing receptor–G-protein complex, allowing the Gα–Gβγ interface to open and to allow GDP exit from the Gα subunit.

Application of proteomic approaches to the GPCR field showed that GPCRs, in addition to G proteins, can interact with multiple intracellular regulatory proteins further extending the questions of the stoichiometry and architecture of these signalling complexes (Bockaert *et al*, 2004; Daulat *et al*, 2009; Ritter and Hall, 2009). Regulators of G-protein signalling (RGS) are GTPase-activating proteins (GAPs) that bind to the activated form of Gα and accelerate its GTPase activity, thereby modulating G-protein signalling (Neitzel and Hepler, 2006; Xie and Palmer, 2007). RGS proteins are a family of highly diverse, multifunctional signalling proteins that share a conserved 120–130 amino-acid core domain (RGS domain), which is responsible for the GAP activity. Several observations indicate that RGS proteins regulate G-protein-dependent signalling not only in a G-protein-specific manner, but also in a receptor-specific manner (Zeng *et al*, 1998; Xu *et al*, 1999; Wang *et al*, 2002; Hague *et al*, 2005). There is increasing evidence for the existence of GPCR protein complexes containing RGS and G proteins (Bernstein *et al*, 2004; Benians *et al*, 2005; Hague *et al*, 2005; Wang *et al*, 2005; Abramow-Newerly *et al*, 2006; Neitzel and Hepler, 2006). However, the molecular architecture and stoichiometry of these complexes are poorly understood.

Here, we used the melatonin MT_1 receptor, a typical G_i-coupled receptor (Jockers *et al*, 2008), as a model to study the molecular architecture of the complex composed of MT_1 homodimers, RGS20 and $G\alpha_i\beta\gamma$ proteins. By searching for specific interacting partners of the MT_1 carboxyl-terminal domain, we previously pulled-down RGS20 from mouse brain lysates (Maurice *et al*, 2008). Interaction between full-length MT_1 and RGS20 was subsequently confirmed in the pituitary *pars tuberalis* (Maurice *et al*, 2008). Here, biochemical, bioluminescence resonance energy transfer (BRET) and electrophysiological approaches were applied to characterize the complex in its basal and agonist-activated state and reveal functional asymmetry of RGS20 and Gi coupling to MT_1 receptors.

Results

RGS20 is part of the pre-existing MT_1 receptor protein complex

To characterize the interaction between MT_1 and RGS20, we performed co-immunoprecipitation experiments by co-expressing Flag-MT_1 or Myc-MT_2 with HA-tagged RGS20 or RGS10 in HEK293T cells (Figure 1A and B). In accordance with previous results (Maurice *et al*, 2008), Flag-MT_1 interacted with HA-RGS20, but not with the related HA-RGS10 in both resting and melatonin (MLT)-activated cells. The second melatonin receptor subtype, MT_2, did not bind to HA-RGS10, whereas low levels of binding were detected for HA-RGS20 (Figure 1A and B). The interaction between MT_1 and RGS20 was further confirmed by BRET in intact HEK293T cells. BRET donor saturation curves were generated by co-expressing constant amounts of the previously described MT_1–Rluc fusion protein (energy donor) (Ayoub *et al*, 2002) and increasing quantities of C-terminally YFP-tagged RGS20 (RGS20-YFP, energy acceptor) (Figure 1D). A specific interaction between these two proteins was indicated by the hyperbolic and saturable behaviour of the BRET donor saturation curve. Stimulation of cells with MLT did not alter BRET signals. Similar results were obtained with a N-terminally YFP-tagged RGS20 (YFP-RGS20) construct (not shown). In contrast, co-expression of MT_1–Rluc with RGS10-YFP expressed at similar levels to those of RGS20-YFP showed non-specific BRET signals (Figure 1D). Similar negative results were obtained with an RGS7-YFP construct (not shown). Taken together, these data show that RGS20 is part of a pre-existing MT_1-associated protein complex for which no further RGS20 recruitment is observed upon MLT stimulation.

RGS20 regulates MT_1-dependent Kir3 channel activation

To establish the functional significance of the MT_1/RGS20 interaction, we studied the effect of MT_1 and RGS20 on the activation of Kir3-type K^+ channels (also designated as GIRKs), which is mediated by the Gβγ subunits of the activated G proteins (Jiang *et al*, 1995; Nelson *et al*, 1996). Application of MLT to $MT_1/Kir_{3.1/3.2}$-expressing CHO cells evoked Ba^{2+}-sensitive outward currents reverting at potentials close to K^+ equilibrium potential (-101.5 ± 1.7 mV, $n = 4$), indicating the activation of Kir3 channels (Dascal, 1997) (Figure 2A and B). RGS20 significantly accelerated the onset of MLT-induced K^+-current responses, similarly to RGS10 that does not bind to MT_1, but activates $G\alpha_i$ proteins (Figure 2A and E). Similarly, the latency between MLT application and signal onset was shortened in cells expressing RGS10 or RGS20 (Supplementary data 1). These kinetic effects are expected to result from the RGS-mediated increase in GTPase activity of $G\alpha_i$ and/or from RGS GAP activity-independent enhancement of coupling between MT_1 and Kir3 channels (Doupnik *et al*, 1997; Jeong and Ikeda, 2001). After fast removal of MLT, Kir3 channels deactivated with strikingly slow time course, most likely reflecting the slow dissociation of MLT from the receptor (Figure 2B and F). RGS10, but not RGS20, significantly decreased the half-decay time of Kir3 channels upon MLT withdrawal (Figure 2B and F) similar to the previously reported effect of RGS4 on MT_1 desensitization (Witt-Enderby *et al*, 2004). In agreement with our data, differential effects of RGS proteins on activation and deactivation kinetics have been reported earlier for several RGS–GPCR couples (Benians *et al*, 2005). To verify that the preventive effect of RGS20 on Kir3 channel deactivation is specific to MT_1 and is not an intrinsic property of RGS20, we studied the activation of Kir3 channels in CHO cells stably expressing the G_i protein-coupled MT_2 receptor. In contrast to MT_1, RGS10 and RGS20 had identical effects on the onset of MLT-induced K^+-current responses and the half-time of channel deactivation in these cells (Figure 2C, E and F) indicating that the effect of RGS20 on channel deactivation is specific for MT_1. Altogether, these results show that MT_1 activates Kir3 channels and that activation kinetics are accelerated by RGS20 consolidating the functional interaction

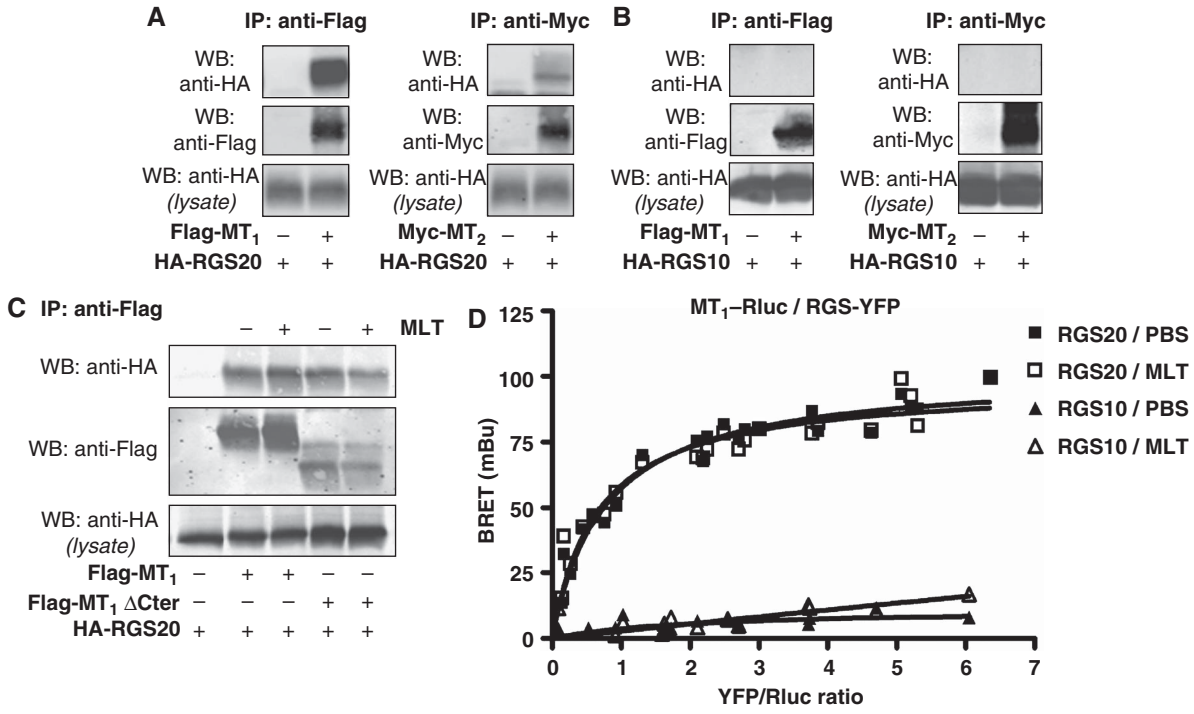

Figure 1 RGS20 constitutively interacts with MT_1. (**A**) Western blots showing co-immunoprecipitation of HA-RGS20 with Flag-MT_1 and weak co-immunoprecipitation with Myc-MT_2 in HEK293T cells. (**B**) Absence of co-immunoprecipitation of HA-RGS10 with Flag-MT_1 and Myc-MT_2. (**C**) Constitutive co-immunoprecipitation of HA-RGS20 with both Flag-MT_1 and Flag-$MT_1\Delta$Cter from HEK293T cells stimulated, or not with MLT (1 μM, 15 min). Data are representative of three experiments. (**D**) BRET donor saturation curves were generated in HEK293T cells expressing a fixed amount of MT_1–Rluc and increasing amounts of RGS20-YFP or RGS10-YFP. Cells were pre-incubated with MLT (1 μM, 10 min) (white square or triangle) or not (black square, triangle). Curves obtained for RGS20-YFP were best fitted with a non-linear regression equation assuming a single-binding site. Curves represent three to five individual saturation experiments.

between RGS20 and MT_1. Differences observed between RGS10 and RGS20 in the half-decay time of Kir3 channel deactivation are most likely due to differences between the direct (RGS20) and indirect (RGS10), through $G\alpha_i$ proteins, coupling to MT_1.

RGS20 binds directly to the Cter and i3 loop of MT_1

RGS20 and MT_1 are known to interact with $G\alpha_i$ subunits (Wang *et al*, 1998; Brydon *et al*, 1999). To determine whether RGS20 binds directly or indirectly (through $G\alpha_i$) to MT_1, we performed pull-down experiments using a chemically synthesized His_6-tagged peptide encompassing the entire MT_1-Cter that was immobilized on Ni-NTA agarose beads. The corresponding MT_2-Cter peptide was used as a negative control. As the third intracellular (i3) loop has been shown to be involved in RGS binding for several other GPCRs (Bernstein *et al*, 2004; Hague *et al*, 2005; Georgoussi *et al*, 2006), we also included the MT_1-i3 loop in our study. As shown in Figure 3A, purified HA-RGS20 specifically binds to the MT_1-Cter and -i3 loop, but only marginally to the MT_2-Cter. The existence of additional binding sites for RGS20 within MT_1 (i3 loop) is consistent with co-immunoprecipitation experiments using a Cter deletion mutant of MT_1, which precipitated less, but still significant amounts of HA-RGS20 compared with full-length MT_1 (Figure 1C).

To identify the minimal-binding motif within the MT_1-Cter, we first designed three truncated MT_1-Cter peptides based on its predicted secondary structure (Figure 3B). Only the full-length peptide was able to efficiently pull-down purified HA-RGS20, suggesting that the membrane-proximal 18 amino acids of the MT_1-Cter, corresponding to the predicted helix 8 (H8), are necessary for HA-RGS20 binding. This hypothesis was confirmed with a synthetic peptide corresponding to H8, which retained similar amounts of purified HA-RGS20 as the full-length peptide (Figure 3B). To determine RGS domains involved in MT_1 binding, we tested the binding capacity of the C-terminal part, encompassing the RGS box (RGS20-box), and the N-terminal part (RGS20-Nter), which was shown to be important for GPCR binding of other RGS proteins (Zeng *et al*, 1998; Bernstein *et al*, 2004; Hague *et al*, 2005; Leontiadis *et al*, 2009). Whereas the RGS20-Nter interacted in pull-down experiments with immobilized His_6-tagged MT_1-Cter and the MT_1-i3 loop peptides, the RGS20-box bound only to the MT_1-Cter (Figure 3C). Neither the RGS20-Nter nor the RGS20-box bound to the truncated MT_1-Cter peptides (Supplementary data 2). Taken together, these results show that RGS20 directly interacts by its Nter domain with the MT_1-i3 loop and by its Nter and Cter domains with the membrane-proximal H8 of the MT_1-Cter.

Molecular dynamics of the $MT_1/RGS20/G_i$ ternary complex monitored by BRET

These results show that RGS20 directly and constitutively interacts with at least two intracellular domains of MT_1. Our previous studies have shown that G_i proteins are also constitutively pre-coupled to MT_1 (Roka *et al*, 1999; Guillaume *et al*, 2008; Maurice *et al*, 2008), raising the question of the molecular organization of RGS20 and G_i in the MT_1 complex.

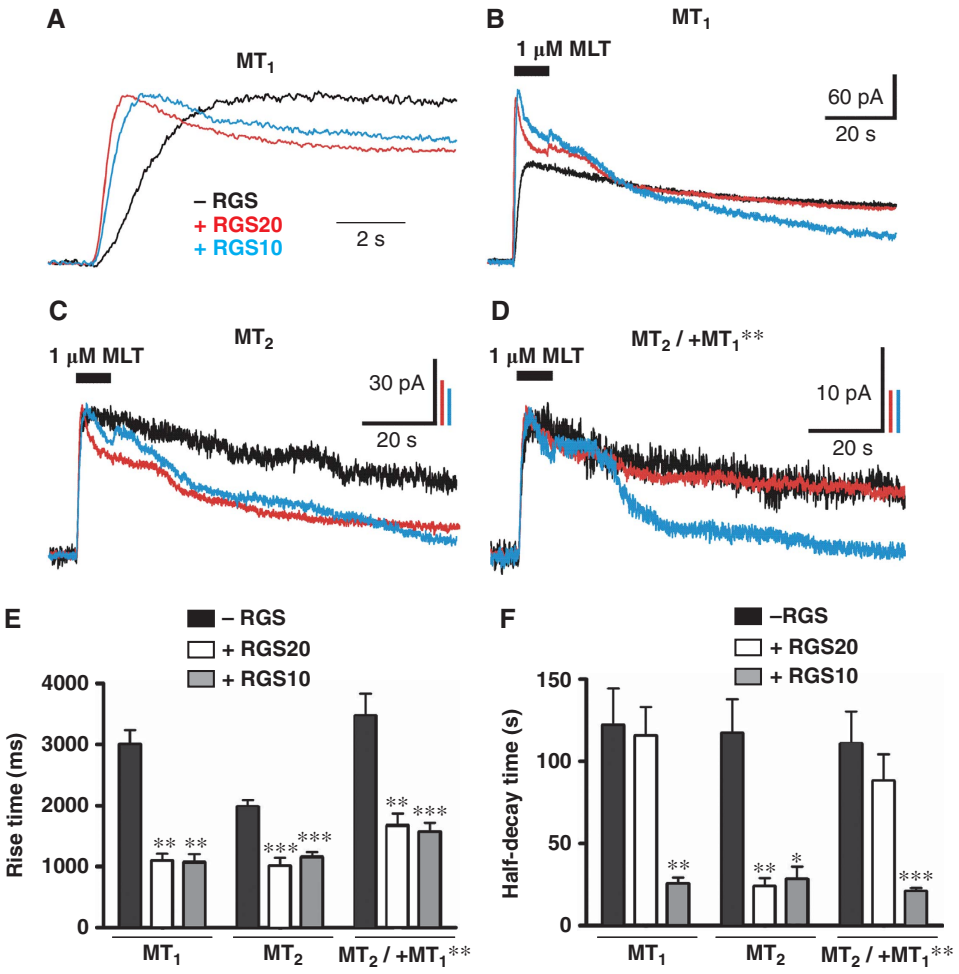

Figure 2 Effect of RGS proteins on MLT-promoted Kir3 channel function. (**A–D**) K^+ currents evoked by 10 s-long fast applications of 1 μM MLT to CHO-cells clamped at −50 mV and stably expressing either MT_1 (**A**, **B**) or MT2 (**C**, **D**) and transiently transfected with $K_{ir}3.1/3.2$ channels (**A–D**), MT1** (**D**) and indicated RGS proteins. (**A**) Expanded time scale of K^+-current traces as in (**B**), emphasizing that RGS proteins speed up the onset of the response. (**E**) Summary bar graph showing that RGS proteins accelerate the activation of receptor-mediated responses; data are mean ± s.e.m. of 10–21 (MT_1), 5–10 (MT_2) and 6–11 (MT_2/MT_1**) experiments. The onset of the K^+-current response is given as 10–90% rise time. Rise time values from RGS20 and RGS10 groups were compared with values in the absence of RGS by Dunnett's Multiple Comparison Test. (**F**) Bar graph summarizing deactivation kinetics of receptor responses expressed as half-decay time of the current after MLT removal. Data are mean ± s.e.m. of 10–11 (MT_1), 4–8 (MT_2) and 6–7 (MT_2/MT_1**) experiments. Half-decay time values from RGS20 and RGS10 groups were compared with values in the absence of RGS by Dunnett's Multiple Comparison Test. The half-decay time values obtained from MLT responses of MT_1 or MT_2/MT_1**-expressing cells transfected with RGS10 were significantly lower compared with the values obtained from RGS20 transfected or untransfected cells. $^*P<0.05$; $^{**}P<0.01$; $^{***}P<0.001$.

We performed BRET experiments to study the molecular proximity of RGS20 and G_i proteins in the presence of MT_1 in intact cells. HEK293 cells stably expressing MT_1 were co-transfected with previously described $G\alpha_{i1}$–Rluc fusion proteins (Galés *et al*, 2006) for which the BRET energy donor Rluc was inserted at two different positions within $G\alpha_{i1}$ ($G\alpha_{i1}$–91-Rluc, $G\alpha_{i1}$–122-Rluc, see Figure 6 for structural details of insertion sites) and with N- or C-terminally YFP-tagged RGS20 fusion proteins (Figure 4A). High BRET signals were detected for all $G\alpha_{i1}$/RGS20 combinations, whereas low BRET signals were obtained with non-fused YFP, expressed at similar levels, defining the background signal of the assay. Differences in BRET signals at equivalent expression levels of different $G\alpha_{i1}$–Rluc and YFP-tagged RGS20 fusion proteins are consistent with the different insertion positions of the Rluc and YFP molecular probes, representing different degrees of molecular proximity. To determine the fraction of the BRET signal that is receptor dependent, we pre-treated cells with pertussis toxin (PTX) at 10 ng/ml, a concentration that abolished the inhibitory effect of MLT on the adenylyl cyclase pathway (Supplementary data 3). ADP-ribosylation of $G\alpha_i$ subunits by PTX uncouples $G\alpha_i$ proteins from GPCRs and thus is expected to move $G\alpha_i$ away from MT_1-bound RGS20 proteins. PTX treatment indeed decreased BRET signals for all $G\alpha_i$/RGS20 combinations, thus revealing the component of the RGS20/$G\alpha_i$ interaction that is receptor dependent.

To study the effect of MLT stimulation of MT_1 on the molecular proximity of RGS20 and $G\alpha_{i1}$ within the complex, BRET donor saturation curves were performed. Cells stably expressing, or not, MT_1 were co-transfected with increasing quantities of RGS20-YFP and a fixed amount of $G\alpha_{i1}$–122-Rluc, a fusion protein previously shown to be sensitive to receptor stimulation (Galés *et al*, 2006). A BRET signal was detected in the absence of MT_1 ($BRET_{max} = 105 \pm 8$, $BRET_{50} = 0.88 \pm 0.20$) (Figure 4B). This signal was insensitive to MLT and PTX incubation (data not shown). In cells

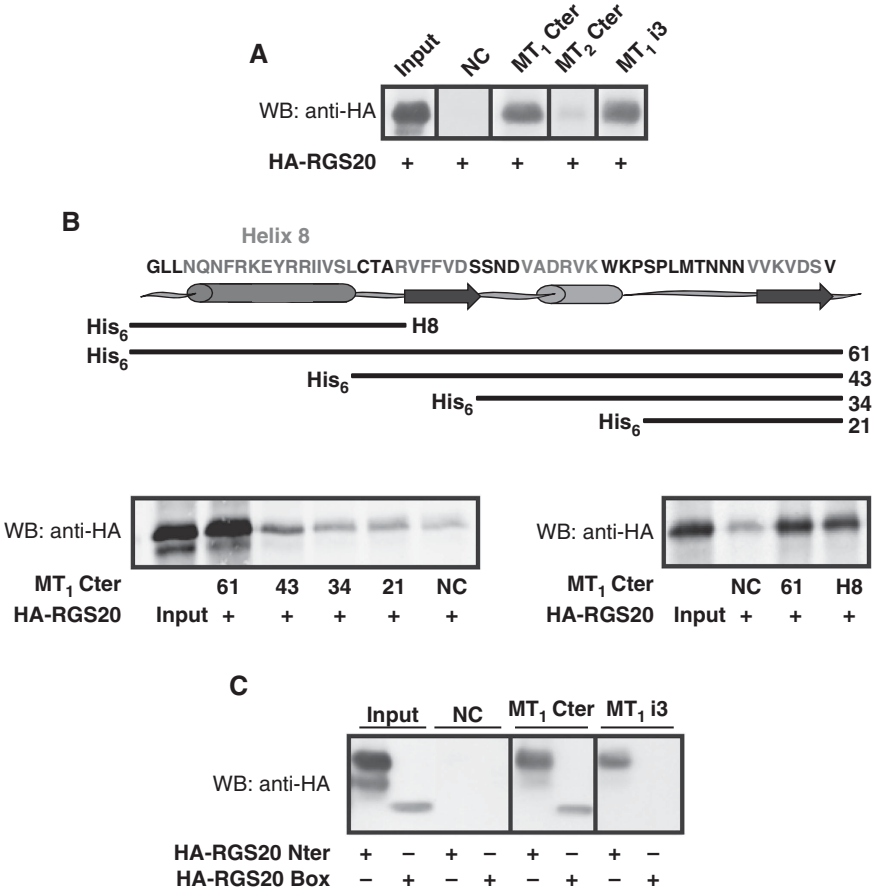

Figure 3 RGS20 binds directly and selectively to the i3 loop and the membrane-proximal helix 8 (H8) of the MT_1-Cter. Synthesized His_6-MT_1-Cter, His_6-MT_1-i3 loop, His_6-MT_2-Cter and truncated versions of His_6-MT_1-Cter peptides (35 nmol) were immobilized on Ni-NTA agarose beads and pull-down experiments were performed using purified (**A**, **B**) full-length HA-RGS20 or (**C**) HA-RGS20-Nter (Nter domain) or HA-RGS20-box (Cter domain). NC, non-coated beads (negative control). Data are representative of three experiments. A full-colour version of this figure is available at *The EMBO Journal* Online.

expressing MT_1, and the same amount of $G\alpha_{i1}$–122-Rluc, the BRET signal was significantly increased ($BRET_{max} = 140 \pm 6$) and the $BRET_{50}$ decreased ($BRET_{50} = 0.11 + 0.02$), indicating an increased propensity of interaction between RGS20 and $G\alpha_i$ in the presence of MT_1 (Figure 4B and C). Data presented in Figure 4C are expressed as percentage of $BRET_{max}$ to better illustrate the shift in $BRET_{50}$. Stimulation with MLT further increased the $BRET_{max}$ ($BRET_{max} = 192 \pm 7$) between $G\alpha_{i1}$–122-Rluc and RGS20-YFP without affecting the $BRET_{50}$ ($BRET_{50} = 0.09 \pm 0.02$) (Figure 4B and C). As previously shown (Mercier *et al*, 2002; Couturier and Jockers, 2003), a change in the $BRET_{max}$ without a shift in $BRET_{50}$ upon agonist stimulation is indicative of conformational rearrangements between interacting proteins, $G\alpha_{i1}$ and RGS20 in our case, and not of additional recruitment. Importantly, in cells expressing similar levels of the G_i-coupled MT_2 receptor, the BRET signal between $G\alpha_{i1}$–122-Rluc and RGS20-YFP was not increased upon MLT stimulation (Figure 4D), showing specificity towards the receptor. The MLT-promoted BRET observed in MT_1-expressing cells was dose dependent (Figure 4E) with an EC_{50} in the subnanomolar range (0.28 nM) that is in agreement with the IC_{50} value of MLT for the inhibition of the adenylyl cyclase pathway (Petit *et al*, 1999). As expected, the MT_1 antagonist luzindole did not increase the basal BRET signal, showing that the MLT-induced BRET correlates with receptor activation (Supplementary data 4). The BRET signal was specific for the $G\alpha_i$ protein as no MLT-induced BRET was observed between RGS20-YFP and a $G\alpha_q$–Rluc fusion protein in MT_1-expressing cells (Supplementary data 5A). The functionality of this G_q probe was assessed in an assay in which angiotensin II induced a BRET decrease in cells co-expressing $G\alpha_q$–97-Rluc and GFP10-$G\gamma_2$ in the presence of the angiotensin II (AT1) receptor (Supplementary data 5B).

These data show that RGS20 and $G\alpha_i$ are part of a constitutive protein complex organized around MT_1 and subjected to conformational rearrangements after MT_1 stimulation. To further characterize these molecular rearrangements, we inserted molecular Rluc and YFP probes at different sites of the MT_1/RGS20/G_i ternary complex and monitored MLT-induced BRET signals. There were no detectable rearrangement between MT_1–Rluc and YFP-RGS20 or RGS20-YFP (Figure 5A) nor intra-molecular rearrangements within RGS20 as monitored by Rluc–RGS20-YFP and YFP-RGS20–Rluc fusion proteins in cells expressing MT_1 (Figure 5B and C). The relative movement between RGS20 and $G\alpha_{i1}$ upon agonist stimulation was detected in cells co-expressing either RGS20-YFP or YFP-RGS20 and $G\alpha_{i1}$–122-Rluc or $G\alpha_{i1}$–91-Rluc constructs (Figure 5D and E). The interaction between RGS20 and $G\alpha_{i1}$–Rluc fusion proteins was confirmed by co-immunoprecipitation experiments in cells expressing MT_1 (Figure 5F). MLT stimulation did not increase the

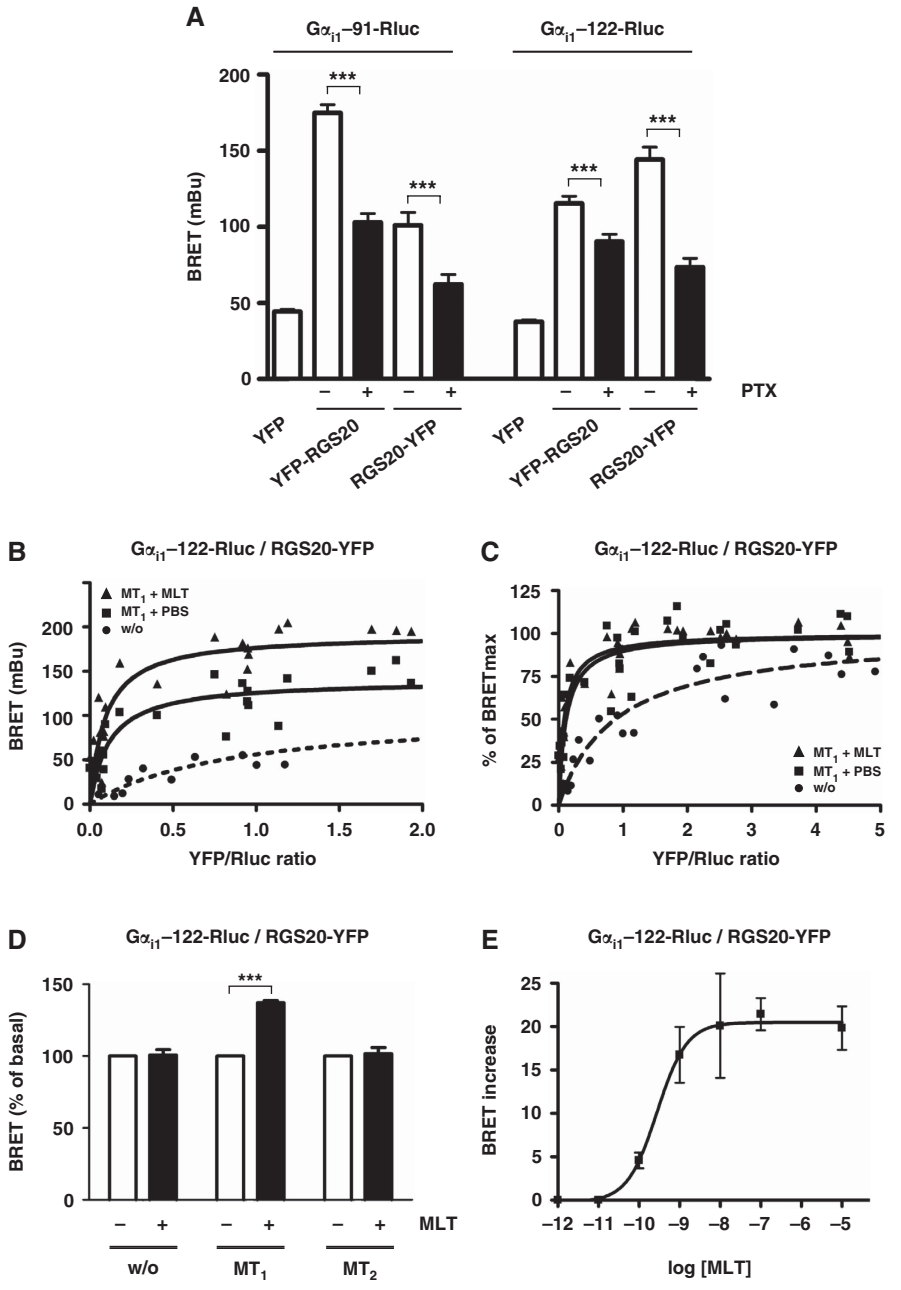

Figure 4 Molecular dynamics of the $MT_1/G_i/RGS20$ complex monitored by BRET in living cells. (**A**) Comparison of BRET between different $G\alpha_{i1}$–Rluc fusion proteins and YFP-RGS20 or RGS20-YFP at $BRET_{max}$ conditions in HEK293 cells stably expressing MT_1. Pertussis toxin (PTX) (10 ng/ml) was used to discriminate between receptor-dependent and -independent effects, and soluble YFP (at equivalent YFP levels) was used as negative control. Data are mean ± s.e.m. of three experiments. (**B**) BRET donor saturation curves were generated in non-transfected HEK293T cells (black circle) or HEK293 cells stably expressing Flag-MT_1 (black triangle, black square) by expressing constant amounts of $G\alpha_{i1}$–122-Rluc and increasing amounts of RGS20-YFP. Cells were incubated with MLT (1 μM, 10 min) (triangle) or not (circle, square) before BRET measurements. Curves represent three to five individual saturation experiments and were best fitted with a non-linear regression equation assuming a single-binding site. (**C**) Normalization of BRET donor saturation curves presented in (**B**) to their respective $BRET_{max}$. (**D**) Comparison of MLT-induced BRET between $G\alpha_{i1}$–122-Rluc and RGS20-YFP at $BRET_{max}$ conditions in wild-type HEK293T (w/o), MT_1 or MT_2 stably expressing HEK293 cells. (**E**) MLT dose–response curve of ligand-induced BRET between $G\alpha_{i1}$–122-Rluc and RGS20-YFP in HEK293 cells stably expressing MT_1. Data are mean ± s.e.m. of three experiments. $^{***}P<0.001$.

amount of precipitated $G\alpha_{i1}$—Rluc, indicating that the MLT-promoted BRET signal shown in Figure 5E corresponds to molecular arrangements within the complex itself rather than additional recruitment. Movement of positions 91 and 122 within the G_i protein is in agreement with the recently described activatory switch of the α-helical domain of the GTPase domain of Gα (Galés *et al*, 2006). Furthermore, MLT stimulation of cells co-expressing MT_1, $G\alpha_{i1}$–122-Rluc and the previously described YFP-Gγ2 fusion protein led to the expected decrease of the BRET signal most likely reflecting the movement of the α-helical domain of $G\alpha_i$ away from the N-ter of Gγ (Figure 5G). A similar decrease was observed in the presence of RGS20, indicating that binding of RGS20 to MT_1 does not interfere with this activatory switch of $G\alpha_i$.

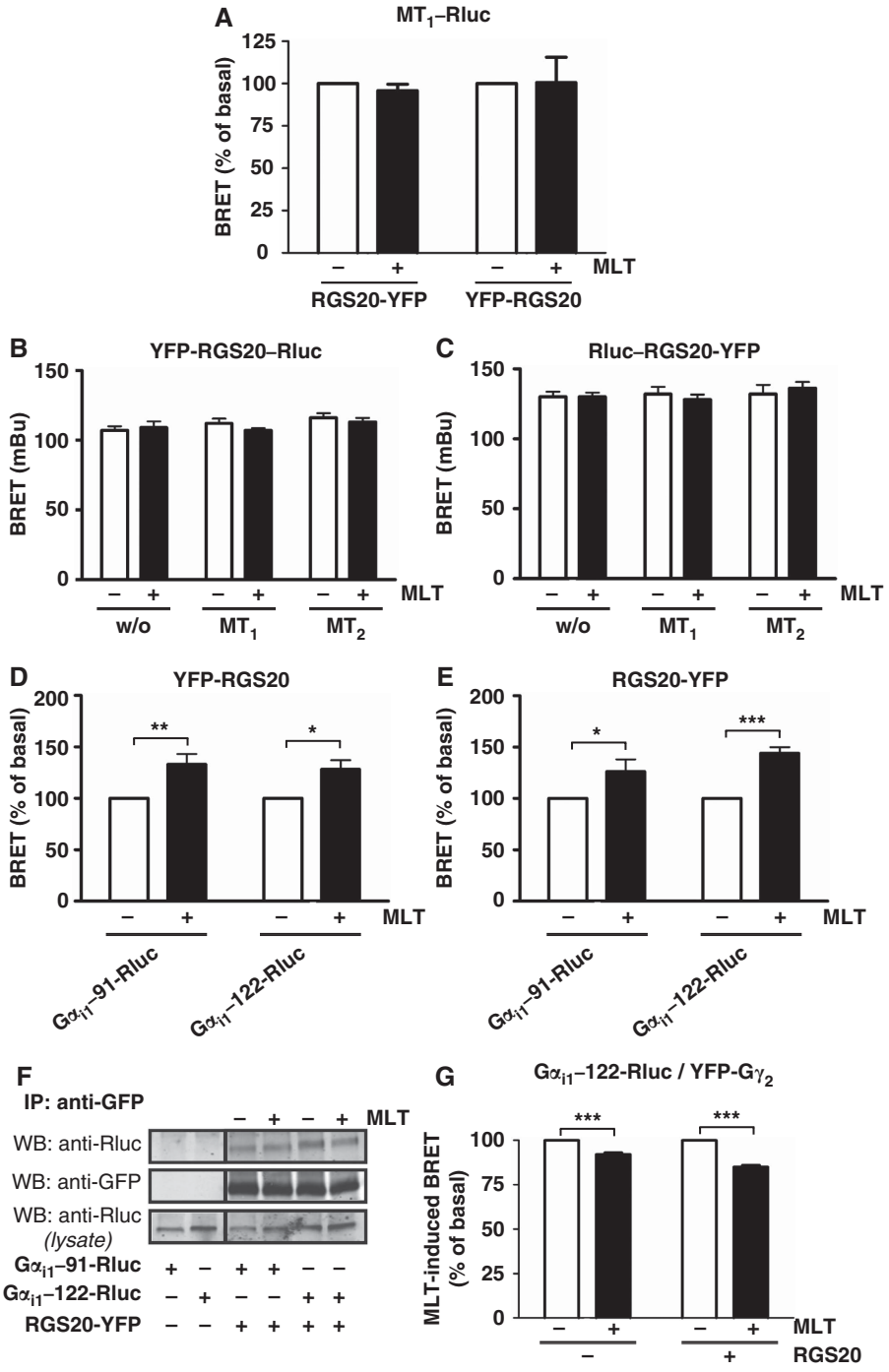

Figure 5 Molecular dynamics of the MT_1/G_i/RGS20 complex monitored by BRET upon MLT stimulation. (**A**) Comparison of MLT-induced BRET between MT_1–Rluc and RGS20-YFP or YFP-RGS20 at $BRET_{max}$ conditions in HEK293T cells. (**B**, **C**) Effects of MLT stimulation on the structural conformation of RGS20 by measuring BRET of YFP-RGS20–Rluc or Rluc–RGS20-YFP in HEK293 cells stably expressing, or not (w/o), MT_1 or MT_2. (**D**, **E**) Comparison of MLT-induced BRET between different $G\alpha_{i1}$–Rluc fusion proteins and (**D**) YFP-RGS20 or (**E**) RGS20-YFP at $BRET_{max}$ conditions in HEK293 cells stably expressing MT_1. (**F**) Western blots showing constitutive co-immunoprecipitation of $G\alpha_{i1}$–Rluc fusion proteins with RGS20-YFP from HEK293 stably expressing MT_1 and stimulated, or not, with MLT. Data are representative of three experiments. (**G**) Effect of RGS20 and MLT stimulation on BRET between $G\alpha_{i1}$–122-Rluc and YFP-$G\gamma_2$ at $BRET_{max}$ conditions in HEK293 cells stably expressing MT_1. MLT was used at 1 μM for 15 min and all data are mean ± s.e.m. of three to five experiments. $^*P<0.05$; $^{**}P<0.01$; $^{***}P<0.001$.

RGS20 and G_i bind to separate receptor protomers in the MT_1/RGS20/G_i complex

Our biochemical and BRET experiments suggest the formation of a constitutive ternary MT_1/RGS20/G_i complex in the basal state with direct interactions of RGS20 and G_i with the MT_1 receptor. The high-resolution crystal structure of several GPCRs and G_i proteins have been solved and a molecular model of the relative position of these two proteins has been proposed based on extensive biochemical evidence (Lambright *et al*, 1996; Liang *et al*, 2003; Fotiadis *et al*,

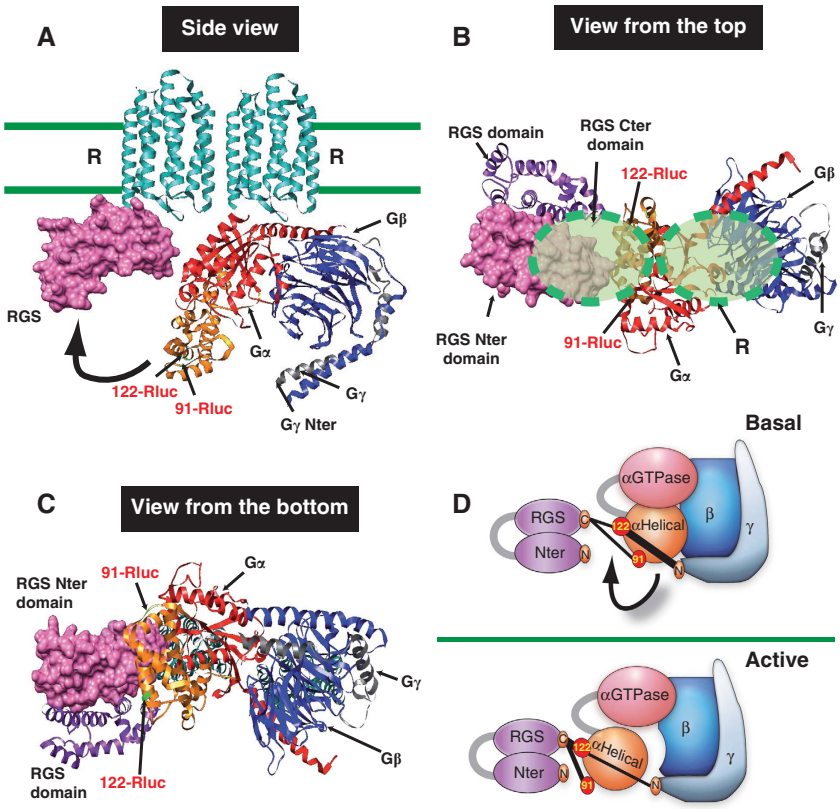

Figure 6 Model of asymmetric organization of the $MT_1/G_i/RGS20$ protein complex at the basal and MLT-stimulated state. (**A–C**) Schematic representation of the complex between a GPCR dimer, the heterotrimeric G protein and RGS. The crystal structures of the $G\alpha_{i1}$-GDP-bound-$G\beta_1\gamma_2$ (PDB entry 1GP2) and the RGS domain of the $G\alpha_{i1}$-GDP-AlF^-_4-RGS4 complex (PDB entry 1AGR) are superposed. The $G\alpha_{i1}$ subunit is shown in red and amber (GTPase domain), $G\beta_1$ in blue, $G\gamma_2$ in grey, the RGS domain is purple and the putative RGS Nter domain is pink. Arrows indicate the positions of Rluc or GFP probes in the $G\alpha_{i1}\beta_1\gamma_2$ heterotrimer. (**D**) Schematic representation of structural rearrangement within the $MT_1/G_i/RGS20$ protein complex detected by BRET after receptor activation by MLT. The colouring is as in (**A**). Following receptor activation, the opening of the $G\alpha_{i1}$ GTPase and helical domain (Galés *et al*, 2006) shortens the distance between the $G\alpha_{i1}$-helical domain (Rluc-91 and -122) and both RGS (N- and C-terminus) while increasing the distances between the $G\alpha_{i1}$-helical domain (Rluc-91 and -122) and $G\gamma_2$ (N-terminus).

2004; Preininger and Hamm, 2004; Rosenbaum *et al*, 2009). Although the crystal structure of RGS20 is currently unknown, the structure of the RGS domain has been solved for several other RGS proteins and appeared to be highly conserved (Tesmer *et al*, 1997; deAlba *et al*, 1999; Soundararajan *et al*, 2008). In addition to the RGS domain, RGS20 contains a large N-terminal domain of similar size. Considering the spatial constrains imposed by the simultaneous presence of $G\alpha_i$, $G\beta$ and $G\gamma$ subunits in proximity to one receptor protomer, direct binding of RGS20 to the same receptor protomer is difficult to reconcile because of the limited space of the intracellular interface of GPCRs (approximately 45 Å diameter). We, therefore, propose that G_i and RGS20 are binding to two different protomers of a receptor dimer (Figure 6). Agonist activation of MT_1 decreased BRET values between $G\alpha_{i1}$–122-Rluc and YFP-$G_{\gamma 2}$ (Figure 5G) in agreement with the previous proposed movement driving $G\alpha$ and $G\beta\gamma$ apart to allow GDP release from the $G\alpha$ subunit after G-protein activation (Galés *et al*, 2006). At the same time, MLT-induced BRET signals are increased between $G\alpha_{i1}$–122-Rluc (and $G\alpha_{i1}$–91-Rluc) and YFP-tagged RGS20 fusion proteins (Figure 5D and E). The simplest explanation for this is a movement of the α-helical domain of $G\alpha$ towards the N-ter of RGS20. Similar results were obtained with both N-terminally and C-terminally YFP-tagged RGS20, suggesting that both extremities are most likely oriented in the same direction. Figure 6 summarizes our model, based on a GPCR dimer that positions RGS20 close to the α-helical domain of $G\alpha_i$ and opposite to $G\beta\gamma$ to explain the observed MLT-induced BRET changes.

Asymmetric interaction of RGS20 and G_i proteins with MT_1/MT_2 heterodimers

To consolidate our prediction that RGS20 and G_i are binding to two separate receptor protomers, we studied RGS20 and G_i binding to the previously described MT_1/MT_2 heterodimer (Ayoub *et al*, 2004). These heterodimers constitute an interesting model as both MLT receptors are G_i-coupled, but only MT_1 strongly binds to RGS20 as shown in Figure 1A. Accordingly, RGS20 was only weakly co-immunoprecipitated when expressed with MT_2 alone, but readily co-immunoprecipitated by MT_2 in the presence of MT_1, indicating that RGS20 is part of the MT_1/MT_2 heterodimer-associated protein complex (Figure 7A).

We then studied the proximity between RGS20 and $G\alpha_i$ in the presence of the MT_1/MT_2 heterodimer using BRET. To monitor MLT-induced rearrangements between RGS20 and $G\alpha_i$ exclusively in protein complexes associated with the

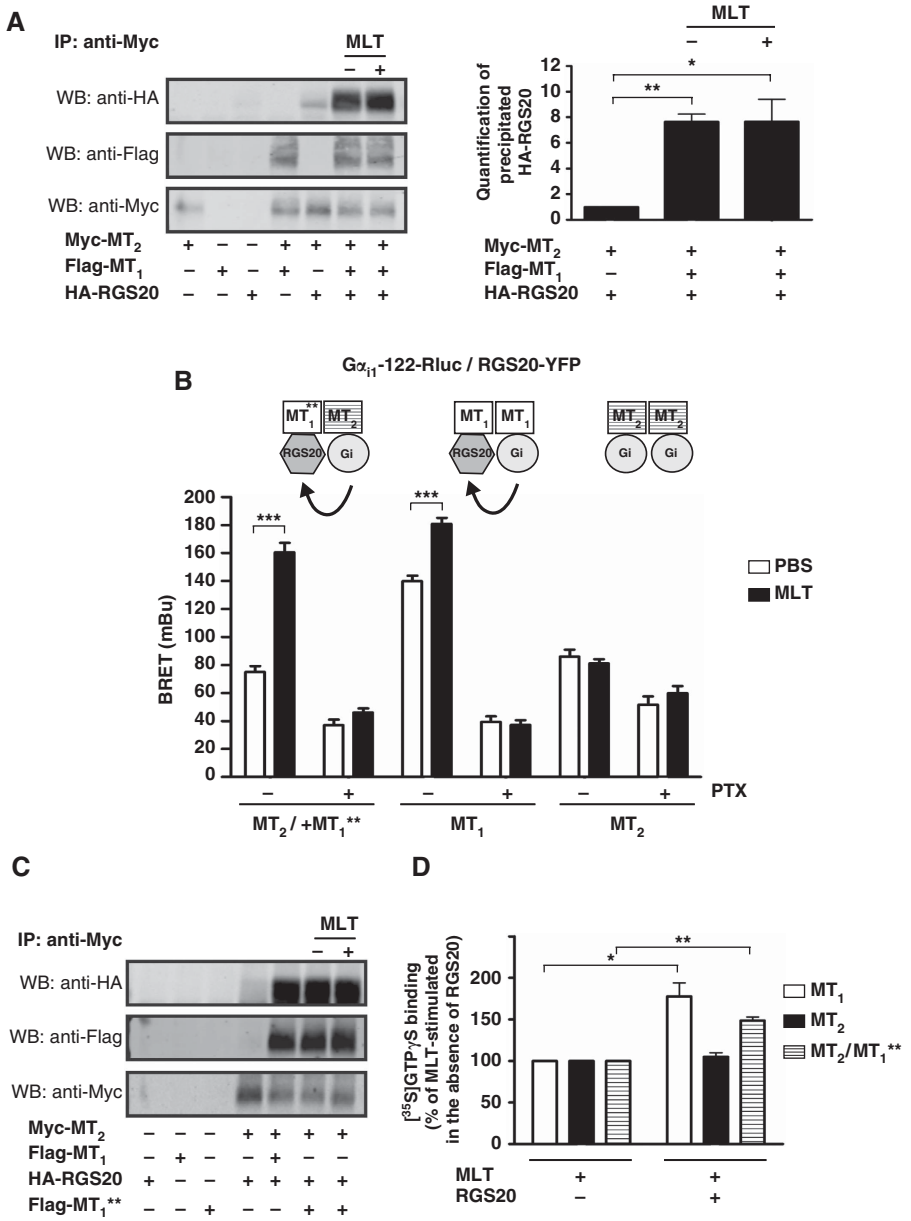

Figure 7 Asymmetric interaction of G_i and RGS20 with MT_1/MT_2 heterodimers. (**A**) Left panel, western blots showing constitutive co-immunoprecipitation of HA-RGS20 with Flag-MT_1/Myc-MT_2 heterodimers from HEK293T cells stimulated, or not, with MLT (1 μM, 15 min). A weak co-immunoprecipitation of HA-RGS20 was observed with Myc-MT_2 alone. Data are representative of three experiments. Right panel, quantification of the amount of immunoprecipitated HA-RGS20 by densitometry analysis. The amount of precipitated HA-RGS20 by Myc-MT2 was normalized at 1. (**B**) Comparison of BRET between $G\alpha_{i1}$–122-Rluc and RGS20-YFP at $BRET_{max}$ conditions (equivalent Rluc and YFP levels) in HEK293 cells expressing the indicated melatonin receptor combination and stimulated (black bar), or not (white bar), by MLT (1 μM, 15 min). Pertussis toxin (PTX) was used at 10 ng/ml. (**C**) Western blots showing constitutive co-immunoprecipitation of HA-RGS20 with Flag-MT_1**/Myc-MT_2 heterodimers from HEK293T cells stimulated or not with MLT (1 μM, 15 min). (**D**) Comparison of [^{35}S]GTPγS binding to MT_1 (white bar)-, MT_2 (black bar)- or MT_2/MT_1** (hatched bar)-expressing CHO cells after MLT stimulation (100 nM, 60 min) in the absence or presence of 0.1 μM purified HA-RGS20. The amount of [^{35}S]GTPγS binding upon MLT stimulation in the absence of HA-RGS20 was normalized at 100. MT_1**; MLT-binding-deficient MT_1 A252C/G258T mutant. All data are mean ± s.e.m. of three to five experiments. $^*P<0.05$; $^{**}P<0.01$; $^{***}P<0.001$.

MT_1/MT_2 heterodimer, we replaced wild-type MT_1 by the previously described MT_1 A252C/G258T mutant (MT_1**), which is devoid of MLT binding (Gubitz and Reppert, 2000). In this configuration, confounding effects of co-expressed MT_1 homodimers on ligand-induced rearrangements between RGS20 and $G\alpha_i$ are excluded, as MT_1 cannot be activated by MLT. Absence of MLT binding and proper cell surface expression of MT_1** was confirmed by 2-[^{125}I]-MLT binding and immunofluorescence microscopy, respectively (Supplementary data 6A and B). Co-immunoprecipitation experiments showed that MT_1** still heterodimerizes with MT_2 and binds to RGS20 (Supplementary data 6C and D). Co-expression of RGS20-YFP and $G\alpha_{i1}$–122-Rluc in cells expressing MT_2/MT_1** heterodimers resulted in a BRET signal that was markedly increased in the presence of MLT, in contrast to cells expressing MT_2 alone, which is consistent with the specific association of RGS20 and $G\alpha_{i1}$ to the MT_2/MT_1** heterodimer (Figure 7B). In cells expressing MT_1 alone, a

similar pattern was observed, although the basal BRET level was higher than in cells expressing either MT_2 homodimers or MT_2/MT_1** heterodimers. PTX pre-treatment decreased basal and MLT-induced BRET signals in cells expressing MT_1 or MT_2/MT_1**, indicating that BRET signals are mainly dependent on the functional interaction of $G\alpha_i$ with receptor homo- and heterodimers. Co-immunoprecipitation experiments showed that the amount of RGS20 bound to the MT_1**/MT_2 heterodimer was not modified by agonist stimulation, indicating that the agonist-induced BRET is due to conformational changes within a pre-existing MT_1**/MT_2/RGS20/G_i complex, as observed for the MT_1/RGS20/G_i complex (Figure 7C). Collectively, our BRET and biochemical data are compatible with the formation of a pre-existing MT_1**/MT_2/RGS20/G_i quaternary complex, wherein the MT_2 protomer can *cis*-activate its $G\alpha_i$ protein and subsequently increase the proximity of $G\alpha_i$ to RGS20 associated to the MT_1** protomer.

To verify whether the recruitment of RGS20 to the MT_1**/MT_2 heterodimer is able to recapitulate the functional consequences of RGS20 expression seen on wild-type MT_1 homodimers (see Figure 2), we expressed the MT_1** mutant in CHO cells stably expressing MT_2. Introduction of MT_1** indeed converted the profile of deactivation seen in cells expressing MT_2 alone (see Figure 2C and E) into an MT_1-like profile in which only RGS10, but not RGS20, decreased the half-decay time of Kir3 channel activation (Figure 2D and F). The effects of RGS10 and RGS20 on rise time and latency of signal onset were all similar to those seen in cells expressing MT_1 and MT_2 alone confirming the functional expression of RGS protein in the MT_1**/MT_2 context (Figure 2E; Supplementary data 1B). This shows that the majority of MT_2 is engaged into MT_1**/MT_2 heterodimers and that the functional effect of RGS20 on Kir3 channel activation by MT_1**/MT_2 heterodimers is similar to that observed for MT_1 homodimers, but different from MT_2 homodimers.

To further explore the functional consequences of RGS20 binding to MT_1, we measured [^{35}S]GTPγS incorporation in CHO cell membranes expressing MT_1, MT_2 or MT_1**/MT_2 in the absence or presence of purified HA-RGS20. Stimulation with MLT induced the expected two- to three-fold increase in [^{35}S]GTPγS binding in all three cell types (not shown). Addition of purified HA-RGS20 into the assay further increased [^{35}S]GTPγS binding in MT_1-expressing membranes, but not in MT_2-expressing membranes (Figure 7D). Importantly, co-expression of the MT_1** mutant in MT_2-expressing cells also enhanced [^{35}S]GTPγS binding, indicating functional coupling of RGS20 proteins to MT_1**/MT_2 heterodimers. Altogether, these data support the functional importance of RGS20 in the MT_1**/MT_2/RGS20/G_i quaternary complex.

Discussion

By using MT_1 homodimers and MT_1/MT_2 heterodimers as model GPCRs, we are extending here two emerging concepts: the pre-assembly of GPCR-interacting complexes and the asymmetric function and organization of GPCR dimers. In addition, we are providing a new functional justification for GPCR dimerization that applies to homo- and heterodimers, namely the possibility of simultaneous and direct binding of GPCR-interacting proteins (GIPs) to the same GPCR dimer composed of two asymmetric protomers. Heterotrimeric G proteins are central, although not exclusive signal transducers of GPCRs. An increasing number of reports suggests the formation of pre-assembled receptor–G-protein complexes, which rearrange upon agonist activation of the receptor (Bunemann *et al*, 2003; Galés *et al*, 2006; Audet *et al*, 2008). This central complex is surrounded by a number of other GIPs that might either compete with the G protein for receptor binding, as in the case of arrestin (Lohse *et al*, 1990), or simultaneously bind to the receptor as shown for the multi-PDZ domain protein MUPP1 (Guillaume *et al*, 2008). Formation of such complexes raises the question of their molecular organization. Although the crystal structure of the GPCR–G-protein complex has not been solved, molecular modelling of the receptor–G-protein interaction based on high-resolution crystal structures of receptors and G proteins alone and biochemical data indicate that the intracellular receptor surface is covered by the heterotrimeric G protein (Arimoto *et al*, 2001; Hamm, 2001; Liang *et al*, 2003; Fotiadis *et al*, 2004) (see also Figure 6). Consequently, small surface accessibility appears difficult to accommodate with simultaneous binding of other GIPs, particularly those that bind to membrane-proximal receptor domains. Formation of receptor signalling units containing distinct GIPs is one possibility to solve this problem. Our data suggest that there might exist at least one other alternative, namely preferential binding of GIPs to the different protomers of GPCR dimers. Given the fact that most GPCRs dimerize, such architecture is likely to be of general importance for GPCR function. This asymmetric model can accommodate binding of GIPs that must be located in the same complex such as G proteins and RGS proteins. The increasing number of examples reporting functional asymmetry of class A and C GPCR dimers is fully compatible with the notion that receptor protomers interact with different GIPs. Several modes of functional cross-talk have been proposed including positive and negative allosteric *trans*- and *cis*-activation within dimers (Pin *et al*, 2005; Sohy *et al*, 2007; Vilardaga *et al*, 2008; Han *et al*, 2009). In the case of *cis*-activation (ligand binding and G-protein activation by the same protomer), the function of the second protomer has remained elusive so far (Damian *et al*, 2008). Our model suggests that the second protomer might function as scaffold to preferentially target GIPs to the receptor dimer. The possible extension of our model towards GPCR oligomers adds further complexity and needs to be explored in the future.

As shown here for the MT_1/RGS20 and MT_1/MT_2/RGS20 complexes, a similar binding mode is likely to occur for several other receptor-RGS pairs. Several studies have reported a direct interaction between RGS proteins and GPCRs (Neitzel and Hepler, 2006). Other studies, which did not address the question of the direct interaction between RGS and receptors, reported implied GPCR–RGS interactions irrespective of the activation state of the receptor (reviewed in Neitzel and Hepler, 2006). The existence of preformed scaffolding complexes containing RGS proteins, G proteins and GPCRs might explain the frequently reported receptor selectivity of RGS proteins.

Preferential asymmetric binding of GIPs to GPCR dimers is fully compatible with the recently proposed model of agonist-induced conformational reorganization within pre-existing receptor–G-protein complexes, reflecting most likely

the proposed movement between Gα and Gβγ required to allow GDP release from the Gα subunit (Galés *et al*, 2006). Indeed, BRET between YFP fusion proteins of RGS20 and $G\alpha_{i1}$–91-Rluc/$G\alpha_{i1}$–122-Rluc was sensitive to agonist stimulation (movement of α-helical domain at positions 91 and 122 of $G\alpha_{i1}$). Insertion of BRET probes at multiple other sites of the complex did not reveal further molecular rearrangements, suggesting a well defined and spatially limited activation mechanism initiated at the level of the ligand-activated receptor and transmitted through the G protein to RGS20. Studies with the MT_1**/MT_2 heterodimer containing a ligand-binding-deficient MT_1 mutant showed that activation of only one receptor protomer is sufficient for G protein *cis* activation, indicating that the function of the MT_2 protomer within the heterodimer is to promote ligand and G-protein binding, whereas the function of the MT_1 protomer is to provide a preferential anchoring site for RGS20. Although we cannot completely exclude the possibility that RGS20 binds directly to MT_2 in the MT_1**/MT_2 heterodimer, this possibility seems unlikely because of the high intrinsic affinity of RGS20 to MT_1 and the MT_1-like signalling profile of MT_1**/MT_2 heterodimers in functional assays.

Our model predicts a binding mode between RGS20 and G_i in a pre-existing complex with a receptor that is different from the spatial organization of the previously reported RGS/$G\alpha_i$ complex (Tesmer *et al*, 1997). The latter complex forms only between the AlF^-_4 activated $G\alpha_i$ subunit and the RGS domain through a binding site partially overlapping with the Gβγ-binding site of $G\alpha_i$. In contrast, binding in the presence of the receptor occurs in the presence of Gβγ and most likely close to the α-helical domain of $G\alpha_i$ and opposite to Gβγ. This model has obviously to be confirmed in further studies, but raises the interesting possibility of a new regulatory mode of G_i by RGS proteins within receptor complexes. Whether MT_1 activation promotes or inhibits RGS20 function in the complex, as might be suggested by the absence of RGS20 activity upon Kir3 channel deactivation, remains to be shown.

In conclusion, we propose a new model highlighting the advantage of GPCRs to be organized as dimers in which each protomer fulfils its specific task by preferentially binding to a specific GIP. This model is fully compatible with the emerging concept of asymmetry within GPCR dimers and may explain receptor specificity of proteins involved in GPCR signalling such as RGS proteins.

Materials and methods

Plasmid constructs

cDNAs encoding human HA-RGS20 and HA-RGS10 were purchased from UMR cDNA Resource Center and pGEX-4T-1 vector from Amersham Pharmacia. The Flag-MT_1, Flag-MT_1ΔCter, Myc-MT_2, MT_1–Rluc and MT_2–Rluc constructs have been described elsewhere (Ayoub *et al*, 2002; Guillaume *et al*, 2008). The cDNAs encoding $G\alpha_{i1}$ was kindly provided by Dr M Ayoub (Montpellier, France) (Ayoub *et al*, 2007) and $G\alpha_{i1}$–91-Rluc, $G\alpha_{i1}$–122-Rluc and YFP-$G\gamma_2$ by Dr M Bouvier (Montreal, Canada) (Galés *et al*, 2006). RGS20-YFP, YFP-RGS20 and RGS10-YFP constructs were obtained using the HA-RGS20 or HA-RGS10 cDNAs as template and the Phusion High-Fidelity DNA Polymerase (Finnzymes). Restriction sites for *Eco*RV and *Xho*I (YFP-RGS20) or *Hind*III and *Bam*HI (RGS20-YFP, RGS10-YFP) were introduced by PCR. After digestion by the respective restriction enzymes, the resulting inserts were ligated into a pcDNA3.1 vector encoding the YFP. The Flag-MT_1 A252C/G258T mutant (MT_1**) was obtained using Flag-MT_1 cDNA as template by PCR-based site-directed mutagenesis in two steps. Briefly, internal primers were used to generate Flag-MT_1 A252C, then Flag-MT_1 A252C/G258T. The YFP-RGS20–Rluc and Rluc–RGS20-YFP constructs were obtained using, respectively, YFP-RGS20 and RGS20-YFP cDNAs as template. Restriction sites for *Hind*III and *Apa*I (YFP-RGS20–Rluc) or *Eco*RV and *Apa*I (Rluc–RGS20-YFP) were introduced by PCR. After digestion by the respective restriction enzymes, the resulting inserts were ligated into a phRluc.N2 (YFP-RGS20–Rluc) or phRluc.C2 (Rluc–RGS20-YFP) plasmid. All DNA sequences were confirmed by sequencing.

Antibodies

Monoclonal anti-HA and anti-GFP antibodies were purchased from Roche Diagnostics. Monoclonal and polyclonal anti-Flag antibodies were from Sigma. Monoclonal and polyclonal anti-Myc and polyclonal anti-$G\alpha_{i3}$ antibodies were purchased from Santa Cruz Biotechnology and monoclonal anti-Rluc from Chemicon.

Cell culture and transfections

Human embryonic kidney 293T (HEK293T) and HEK293 cells stably expressing MT_1 or MT_2 were cultured in Dulbecco's modified Eagle's medium supplemented with 10% (v/v) foetal bovine serum, 100 units/ml penicillin, 0.1 mg/ml streptomycin, 0.02 M Hepes with, or not, 0.4 mg/ml geneticin, at 37°C in a humidified atmosphere at 95% air and 5% CO_2. Transient transfections were performed with FuGENE6 (Roche Molecular Biochemicals) or JET-PEI (Polyplus Transfection), according to the manufacturer's protocol. For electrophysiology experiments, CHO-K1 cells stably expressing human MT_1 or MT_2 were maintained in Ham's F12 Glutamax supplemented with 10% foetal bovine serum, 100 units/ml penicillin, 0.1 mg/ml streptomycin and 0.4 mg/ml geneticin. Transient transfections of concatemers of Kir3.1/3.2 subunits, RGS20, RGS10 and Flag-MT_1** were performed with Lipofectamine 2000 (Invitrogen). For [^{35}S]GTPγS-binding studies, transient transfections of Flag-MT_1** were performed by electroporation using the Amaxa kit T^{TM} (Lonza).

Expression and purification of recombinant proteins

To express HA-RGS20 as a GST fusion protein, restriction sites for *Bam*HI and *Xho*I were introduced immediately adjacent to the initiation and termination codon by PCR of the plasmid encoding HA-RGS20 using the phusion high-fidelity DNA polymerase (Finnzymes). For HA-RGS20-Nter, corresponding to amino-acid (aa) 1–89 of RGS20 (whole sequence 216 aa), a restriction site for *Bam*HI was introduced immediately adjacent to the initiation codon and for *Sal*I after a stop codon by PCR of the HA-RGS20 plasmid. For HA-RGS20-box, corresponding to aa 90–216 of RGS20, the RGS box was sub-cloned in a plasmid encoding amino-terminal HA tag then restriction sites for *Sal*I and *Not*I were introduced immediately adjacent to the initiation and termination codon by PCR. After digestion by their respective restriction sites, the resulting inserts were ligated into pGEX-4T-1 vector. All DNA sequences were confirmed by sequencing. The resulting plasmids were transformed into BL21(DE3) cells (Invitrogen) and cells were grown in LB media containing 50 μg/ml ampicillin. Expression of GST fusion proteins was induced by adding 300 μM to 1 mM isopropylthiogalactoside (Sigma) to mid-log cultures. Cultures were harvested after 5 to 7 h at 37°C and cells centrifuged at 6000 *g* for 15 min. The pellets were re-suspended in cold PBS containing protease inhibitor cocktail EDTA free, crushed with an Ultra-turrax T25 and sonicated. After adding 1% Triton-X100 (Sigma), the cell suspensions were centrifuged at 10 000 *g* for 30 min, the supernatants collected and applied to glutathione-agarose beads (Sigma) that had been equilibrated with 1% Triton-X100 in PBS. After extensive washes, HA-tagged proteins were eluted by 0.04 U/μl of thrombin (Amersham Biosciences) in PBS (2 h, 22°C). Eluates were applied to new freshly glutathione-agarose beads to eliminate residual contaminant GST and bacterial proteins. Purity of HA-tagged proteins was assessed by SDS–PAGE after silver staining.

Electrophysiology

Experiments with CHO-K1 cells stably expressing MT_1 or MT_2 were performed at room temperature (23–24°C) 1–3 days after a transfection with Kir3.1/3.2, RGS20, RGS10 and Flag-MT_1**. Cells were continuously superfused with an extracellular solution composed of (in mM): 145 NaCl, 2.5 KCl, 1 $MgCl_2$, 2 $CaCl_2$, 10 HEPES, 25 glucose; pH 7.3, 323 mosm. Patch pipettes had resistances between 3–4 MΩ when filled with intracellular solution

composed of (in mM) 107.5 potassium gluconate, 32.5 KCl, 10 HEPES, 5 EGTA, 4 MgATP, 0.6 NaGTP, 10 Tris phosphocreatine; pH 7.2, 297 mosm. Series resistance ($<5\,M\Omega$) was compensated by 80%. Melatonin receptor responses were evoked by fast application of MLT and recorded with an Axopatch 200B patch-clamp amplifier; filtering and sampling frequencies were set to 1 and 5 kHz, respectively. The deactivation time course was often not exponential, but exhibited a slight hump that made exponential curve fitting imprecise. Therefore, we quantified the rate of deactivation by measuring the time for the current level at the end of MLT application to drop by 50% (half-decay time). Recording of currents, curve fitting and further data analyses were performed with pClamp software.

BRET measurement

Rluc- and YFP-tagged protein constructs were transiently co-transfected into HEK293T cells or HEK293 cells stably expressing MT_1 or MT_2, seeding in 12-well plates. Twenty-four hours after transfection, cells were trypsinated and 1×10^5 were distributed in a 96-well white Optiplate (PerkinElmer Life Sciences) pre-coated with 10 μg/ml poly-L-lysine (Sigma) for another 24 h. After two washes with PBS, coelenterazine h substrate (Molecular Probes) and MLT (or PBS) were added for 15 min at a final concentration of 5 and 1 μM, respectively. Light-emission acquisition at 485 and 530 nm was then started. The BRET ratio was calculated as the ratio of the emission at 530 over 485 nm of co-transfected 10 ng Rluc-tagged protein and 12.5 to 500 ng YFP-tagged protein. BRET signal values were then corrected by subtracting the background BRET signal detected when the Rluc-tagged protein was expressed alone from the BRET signal detected in cells co-expressing both Rluc- and YFP-tagged constructs. Luminescence and fluorescence were measured simultaneously using the lumino/fluorometer Mithras™ (Berthold) that allows the sequential integration of luminescence signals detected with two filter settings (Rluc filter, 485 ± 10 nm; YFP filter, 530 ± 12.5 nm). Total fluorescence was measured with the fluorometer Fusion™ (Packard Instrument Company). The results were expressed in milliBRET units, 1 milliBRET corresponding to the BRET ratio values multiplied by 1000. In some experiments, PTX (Alexis® Biochemicals) was used to discriminate between receptor-dependent and -independent effects. Cells were incubated with 10 ng/ml PTX in serum-free medium (5 h, 37°C) before BRET measurements.

Immunoprecipitations

HEK293T cells grown in six-well plates were co-transfected with plasmids encoding the indicated constructs. Forty-eight hours after transfection, cells were stimulated, or not, with 1 μM MLT for 15 min at 37°C, washed two times in PBS, and lysed in 500 μl cold lysis buffer (75 mM Tris, 2 mM EDTA, 12 mM $MgCl_2$, 10 mM CHAPS, protease inhibitor cocktail EDTA free, 10 mM NaF, 2 mM Na_3VO_4, pH 7.4). After sonication and solubilization during 3–5 h at 4°C under gentle end-over-end mixing, lysates were centrifuged at 12 000 *g* during 1 h at 4°C. Immunoprecipitations were performed using 2–4 μg of the indicated antibodies pre-adsorbed on protein G sepharose beads (Sigma) for 2 h at 4°C. Immunoprecipitated proteins were eluted with Laemmli buffer and subjected to SDS–PAGE and immunoblotting. Immunoblottings were performed using the indicated antibodies and immunoreactivity was revealed using secondary antibodies coupled to 680 or 800 nm fluorophores using the Odyssey LI-COR infrared fluorescent scanner (ScienceTec).

Pull-down assay

Peptides encompassing the His_6-MT_1-Cter, His_6-MT_1-i3 loop, His_6-MT_2-Cter (NeoMPS) and the His_6-truncated MT_1-Cter (Proteogenix) were chemically synthesized and purified by HPLC (>90% purity). A total of 35 nmol of purified peptides were immobilized on 20 μl Ni-NTA agarose beads (Qiagen) and quantitative immobilization was monitored by measuring the absorbance of the supernatant as previously described (Maurice *et al*, 2008). Beads were incubated with 0.5 μg of purified HA-tagged full-length, Nter or Cter domain of RGS20 in 500 μl of binding buffer (20 mM NaH_2PO_4, 10 mM CHAPS, 150 mM NaCl, 2 mM Na_3VO_4, 10 mM NaF, protease inhibitor cocktail EDTA free, 100 μM GDP, 1 mM AEBSF, 20 mM imidazole, 0.05 % BSA, pH 8) for 2 h at 4°C with gentle shaking. The beads were washed three times with binding buffer, and recruited proteins were eluted with Leammli buffer and subjected to SDS–PAGE and immunoblotting.

[^{35}S]GTPγS binding

CHO cells (2.10^6) stably expressing MT_1 or MT_2 were electroporated using the Amaxa kit T™ with 4 μg of Flag-MT_1** or empty vector (pcDNA3) cDNAs according to manufacturer's specifications. Forty-eight hours after electroporation, [^{35}S]GTPγS binding was determined from crude membranes in 100 μl of reaction mixture containing 20 mM HEPES (pH 7.4), 100 mM NaCl, 3 mM $MgCl_2$, 20 μg/ml saponin, 3 μM GDP, 0.3 nM [^{35}S]GTPγS and purified HA-RGS20 (0.1 μM) with or without 1 μM melatonin. The reaction was started by transferring tubes at room temperature and stopped after 60 min incubation by addition of 1 ml of ice-cold stop buffer containing 10 mM Tris–HCl (pH 8.0), 100 mM NaCl, 20 mM $MgCl_2$, 0.1 mM GTP. Bound and free radioactivity was separated by filtration over GF/F glass fibre filters (Whatman).

GPCR, heterotrimeric G-protein and RGS structure representation

Ribbon diagrams were generated using coordinates from Protein Data Bank files as indicated and visualized with CHIMERA software.

Data and statistical analysis

All data represent the mean ± s.e.m. of three to five independent experiments for biochemical and BRET studies and 4 to 21 for electrophysiology. The results were analysed by PRISM (GraphPad Software Inc.) and statistical significance was assessed by two-way Anova or Student's *t* tests for biochemical and BRET studies or ANOVA with the Dunnett's multiple comparison test for electrophysiology (*$P<$ 0.05; **$P<0.01$; ***$P<0.001$).

Supplementary data

Supplementary data are available at *The EMBO Journal* Online (http://www.embojournal.org).

Acknowledgements

This work was supported by grants from SERVIER, the Fondation Recherche Médicale ('Equipe FRM'), Fondation pour la Recherche sur le Cerveau (FRC) Neurodon, Institut National de la Santé et de la Recherche Médicale (INSERM), Centre National de la Recherche Scientifique (CNRS). RT was supported by the Wellcome Trust International Senior Research Fellowship Award and by a grant from GACR (309/06/1304). BB was supported by the Swiss Science Foundation (3100A0-117816). AMD held an EGID fellowship. We thank Dr Michel Bouvier (University of Montreal) for kindly providing the G-protein Rluc and YFP fusion proteins, Dr Billy Breton (University of Montreal), Dr Julie Dam (Institut Cochin) and Patty Chen (Institut Cochin) for helpful discussions and comments.

Conflict of interest

The authors declare that they have no conflict of interest.

References

Abramow-Newerly M, Roy AA, Nunn C, Chidiac P (2006) RGS proteins have a signalling complex: interactions between RGS proteins and GPCRs, effectors, and auxiliary proteins. *Cell Signal* **18:** 579–591

Arimoto R, Kisselev OG, Makara GM, Marshall GR (2001) Rhodopsin-transducin interface: studies with conformationally constrained peptides. *Biophys J* **81:** 3285–3293

Audet N, Galés C, Archer-Lahlou E, Vallières M, Schiller PW, Bouvier M, Pineyro G (2008) Bioluminescence resonance energy transfer assays reveal ligand-specific conformational changes within preformed signaling complexes containing delta-opioid receptors and heterotrimeric G proteins. *J Biol Chem* **283:** 15078–15088

Ayoub MA, Couturier C, Lucas-Meunier E, Angers S, Fossier P, Bouvier M, Jockers R (2002) Monitoring of ligand-independent dimerization and ligand-induced conformational changes of melatonin receptors in living cells by bioluminescence resonance energy transfer. *J Biol Chem* **277:** 21522–21528

Ayoub MA, Levoye A, Delagrange P, Jockers R (2004) Preferential formation of MT1/MT2 melatonin receptor heterodimers with distinct ligand interaction properties compared with MT2 homodimers. *Mol Pharmacol* **66:** 312–321

Ayoub MA, Maurel D, Binet V, Fink M, Prézeau L, Ansanay H, Pin JP (2007) Real-time analysis of agonist-induced activation of protease-activated receptor 1/Galphai1 protein complex measured by bioluminescence resonance energy transfer in living cells. *Mol Pharmacol* **71:** 1329–1340

Baneres JL, Martin A, Hullot P, Girard JP, Rossi JC, Parello J (2003) Structure-based analysis of GPCR function: conformational adaptation of both agonist and receptor upon leukotriene B4 binding to recombinant BLT1. *J Mol Biol* **329:** 801–814

Bayburt TH, Leitz AJ, Xie G, Oprian DD, Sligar SG (2007) Transducin activation by nanoscale lipid bilayers containing one and two rhodopsins. *J Biol Chem* **282:** 14875–14881

Benians A, Nobles M, Hosny S, Tinker A (2005) Regulators of G-protein signaling form a quaternary complex with the agonist, receptor, and G-protein. A novel explanation for the acceleration of signaling activation kinetics. *J Biol Chem* **280:** 13383–13394

Bernstein LS, Ramineni S, Hague C, Cladman W, Chidiac P, Levey AI, Hepler JR (2004) RGS2 binds directly and selectively to the M1 muscarinic acetylcholine receptor third intracellular loop to modulate Gq/11alpha signaling. *J Biol Chem* **279:** 21248–21256

Bockaert J, Roussignol G, Bécamel C, Gavarini S, Joubert L, Dumuis A, Fagni L, Marin P (2004) GPCR-interacting proteins (GIPs): nature and functions. *Biochem Soc Trans* **32:** 851–855

Bouvier M (2001) Oligomerization of G-protein-coupled transmitter receptors. *Nat Rev Neurosci* **2:** 274–286

Bunemann M, Frank M, Lohse MJ (2003) Gi protein activation in intact cells involves subunit rearrangement rather than dissociation. *Proc Natl Acad Sci USA* **100:** 16077–16082

Brydon L, Roka F, Petit L, de Coppet P, Tissot M, Barrett P, Morgan PJ, Nanoff C, Strosberg AD, Jockers R (1999) Dual signaling of human Mel1a melatonin receptors via G(i2), G(i3), and G(q/11)proteins. *Mol Endocrinol* **13:** 2025–2038

Couturier C, Jockers R (2003) Activation of leptin receptor by a ligand-induced conformational change of constitutive receptor dimers. *J Biol Chem* **278:** 26604–26611

Dascal N (1997) Signalling via the G protein-activated K+ channels. *Cell Signal* **9:** 551–573

Damian M, Mary S, Martin A, Pin JP, Baneres JL (2008) G protein activation by the leukotriene B4 receptor dimer. Evidence for an absence of trans-activation. *J Biol Chem* **283:** 21084–21092

Daulat AM, Maurice P, Jockers R (2009) Recent methodological advances in the discovery of GPCR-associated protein complexes. *Trends Pharmacol Sci* **30:** 72–78

deAlba E, DeVries L, Farquhar MG, Tjandra N (1999) Solution structure of human GAIP (G alpha interacting protein): a regulator of G protein signaling. *J Mol Biol* **291:** 927–939

Doupnik CA, Davidson N, Lester HA, Kofuji P (1997) RGS proteins reconstitute the rapid gating kinetics of gbetagamma-activated inwardly rectifying K+ channels. *Proc Natl Acad Sci USA* **94:** 10461–10466

Ernst OP, Gramse V, Kolbe M, Hofmann KP, Heck M (2007) Monomeric G protein-coupled receptor rhodopsin in solution activates its G protein transducin at the diffusion limit. *Proc Natl Acad Sci USA* **104:** 10859–10864

Fotiadis D, Liang Y, Filipek S, Saperstein DA, Engel A, Palczewski K (2004) The G protein-coupled receptor rhodopsin in the native membrane. *FEBS Lett* **564:** 281–288

Galés C, Rebois RV, Hogue M, Trieu P, Breit A, Hébert TE, Bouvier M (2005) Real-time monitoring of receptor and G-protein interactions in living cells. *Nat Methods* **2:** 177–184

Galés C, Van Durm JJ, Schaak S, Pontier S, Percherancier Y, Audet M, Paris H, Bouvier M (2006) Probing the activation-promoted structural rearrangements in preassembled receptor-G protein complexes. *Nat Struct Mol* **13:** 778–786

George SR, O'Dowd BF, Lee SP (2002) G-protein-coupled receptor oligomerization and its potential for drug discovery. *Nat Rev Drug Discov* **1:** 808–820

Georgoussi Z, Leontiadis L, Mazarakou G, Merkouris M, Hyde K, Hamm H (2006) Selective interactions between G protein subunits and RGS4 with the C-terminal domains of the mu- and delta-opioid receptors regulate opioid receptor signaling. *Cell Signal* **18:** 771–782

Gubitz AK, Reppert SM (2000) Chimeric and point-mutated receptors reveal that a single glycine residue in transmembrane domain 6 is critical for high affinity melatonin binding. *Endocrinology* **141:** 1236–1244

Guillaume JL, Daulat AM, Maurice P, Levoye A, Migaud M, Brydon L, Malpaux B, Borg-Capra C, Jockers R (2008) The PDZ protein mupp1 promotes Gi coupling and signaling of the Mt1 melatonin receptor. *J Biol Chem* **283:** 16762–16771

Hague C, Bernstein LS, Ramineni S, Chen Z, Minneman KP, Hepler JR (2005) Selective inhibition of alpha1A-adrenergic receptor signaling by RGS2 association with the receptor third intracellular loop. *J Biol Chem* **280:** 27289–27295

Hamm HE (2001) How activated receptors couple to G proteins. *Proc Natl Acad Sci USA* **98:** 4819–4821

Han Y, Moreira IS, Urizar E, Weinstein H, Javitch JA (2009) Allosteric communication between protomers of dopamine class A GPCR dimers modulates activation. *Nat Chem Biol* **5:** 688–695

Herrick-Davis K, Grinde E, Harrigan TJ, Mazurkiewicz JE (2005) Inhibition of serotonin 5-hydroxytryptamine 2c receptor function through heterodimerization: receptor dimers bind two molecules of ligand and one G-protein. *J Biol Chem* **280:** 40144–40151

Jeong SW, Ikeda SR (2001) Differential regulation of G protein-gated inwardly rectifying K(+) channel kinetics by distinct domains of RGS8. *J Physiol* **535:** 335–347

Jiang Z, Nelson C, Allen C (1995) Melatonin activates an outward current and inhibits lh in rat suprachiasmatic nucleus neurons. *Brain Res* **687:** 125–132

Jockers R, Maurice P, Boutin JA, Delagrange P (2008) Melatonin receptors, heterodimerization, signal transduction and binding sites: what's new? *Br J Pharmacol* **154:** 1182–1195

Lambright DG, Sondek J, Bohm A, Skiba NP, Hamm HE, Sigler PB (1996) The 2.0 A crystal structure of a heterotrimeric G protein. *Nature* **379:** 311–319

Leontiadis LJ, Papakonstantinou MP, Georgoussi Z (2009) Regulator of G protein signaling 4 confers selectivity to specific G proteins to modulate mu- and delta-opioid receptor signaling. *Cell Signal* **21:** 1218–1228

Liang Y, Fotiadis D, Filipek S, Saperstein DA, Palczewski K, Engel A (2003) Organization of the G protein-coupled receptors rhodopsin and opsin in native membranes. *J Biol Chem* **278:** 21655–21662

Lohse MJ, Benovic JL, Codina J, Caron MG, Lefkowitz RJ (1990) β-arrestin: a protein that regulates β-adrenergic receptor function. *Science* **248:** 1547–1550

Maurice P, Daulat AM, Broussard C, Mozo J, Clary G, Hotellier F, Chafey P, Guillaume JL, Ferry G, Boutin JA, Delagrange P, Camoin L, Jockers R (2008) A generic approach for the purification of signaling complexes that specifically interact with the carboxyl-terminal domain of G protein-coupled receptors. *Mol Cell Proteomics* **7:** 1556–1569

Mercier JF, Salahpour A, Angers S, Breit A, Bouvier M (2002) Quantitative assessment of beta 1 and beta 2-adrenergic receptor homo and hetero-dimerization by bioluminescence resonance energy transfer. *J Biol Chem* **277:** 44925–44931

Milligan G (2009) G protein-coupled receptor hetero-dimerization: contribution to pharmacology and function. *Br J Pharmacol* **158:** 5–14

Milligan G (2010) The role of dimerisation in the cellular trafficking of G-protein-coupled receptors. *Curr Opin Pharmacol* **10:** 23–29

Neitzel KL, Hepler JR (2006) Cellular mechanisms that determine selective RGS protein regulation of G protein-coupled receptor signaling. *Semin Cell Dev Biol* **17:** 383–389

Nelson CS, Marino JL, Allen CN (1996) Melatonin receptors activate heteromeric G-protein coupled Kir3 channels. *Neuroreport* **7:** 717–720

Petit L, Lacroix I, deCoppet P, Strosberg AD, Jockers R (1999) Differential signaling of human Mel1a and Mel1b melatonin receptors through the cyclic guanosine 3′-5′-monophosphate pathway. *Biochem Pharmacol* **58:** 633–639

Pin JP, Kniazeff J, Liu J, Binet V, Goudet C, Rondard P, Prézeau L (2005) Allosteric functioning of dimeric class C G-protein-coupled receptors. *FEBS J* **272:** 2947–2955

Preininger AM, Hamm HE (2004) G protein signaling: insights from new structures. *Sci STKE* **27:** Re3

Ritter SL, Hall RA (2009) Fine-tuning of GPCR activity by receptor-interacting proteins. *Nat Rev Mol Cell Biol* **10:** 819–830

Rivero-Müller A, Chou YY, Ji I, Lajic S, Hanyaloglu AC, Jonas K, Rahman N, Ji TH, Huhtaniemi I (2010) Rescue of defective G protein-coupled receptor function *in vivo* by intermolecular cooperation. *Proc Natl Acad Sci USA* **107:** 2319–2324

Roka F, Brydon L, Waldhoer M, Strosberg AD, Freissmuth M, Jockers R, Nanoff C (1999) Tight association of the human Mel(1a)-melatonin receptor and G(i): precoupling and constitutive activity. *Mol Pharmacol* **56:** 1014–1024

Rosenbaum DM, Rasmussen SG, Kobilka BK (2009) The structure and function of G-protein-coupled receptors. *Nature* **459:** 356–363

Rovira X, Pin JP, Giraldo J (2010) The asymmetric/symmetric activation of GPCR dimers as a possible mechanistic rationale for multiple signalling pathways. *Trends Pharmacol Sci* **31:** 15–21

Sohy D, Parmentier M, Springael JY (2007) Allosteric transinhibition by specific antagonists in CCR2/CXCR4 heterodimers. *J Biol Chem* **282:** 30062–30069

Soundararajan M, Willard FS, Kimple AJ, Turnbull AP, Ball LJ, Schoch GA, Gileadi C, Fedorov OY, Dowler EF, Higman VA, Hutsell SQ, Sundström M, Doyle DA, Siderovski DP (2008) Structural diversity in the RGS domain and its interaction with heterotrimeric G protein alpha-subunits. *Proc Natl Acad Sci USA* **105:** 6457–6462

Tesmer JJ, Berman DM, Gilman AG, Sprang SR (1997) Structure of RGS4 bound to AlF4-activated G(i alpha1): stabilization of the transition state for GTP hydrolysis. *Cell* **89:** 251–261

Vilardaga JP, Nikolaev VO, Lorenz K, Ferrandon S, Zhuang Z, Lohse MJ (2008) Conformational cross-talk between alpha2A-adrenergic and mu-opioid receptors controls cell signaling. *Nat Chem Biol* **4:** 126–131

Wang J, Ducret A, Tu Y, Kozasa T, Aebersold R, Ross EM (1998) RGSZ1, a Gz-selective RGS protein in brain. Structure, membrane association, regulation by Galphaz phosphorylation, and relationship to a Gz gtpase-activating protein subfamily. *J Biol Chem* **273:** 26014–26025

Wang Y, Ho G, Zhang JJ, Nieuwenhuijsen B, Edris W, Chanda PK, Young KH (2002) Regulator of G protein signaling Z1 (RGSZ1) interacts with Galpha i subunits and regulates Galpha i-mediated cell signaling. *J Biol Chem* **277:** 48325–48332

Wang X, Zeng W, Soyombo AA, Tang W, Ross EM, Barnes AP, Milgram SL, Penninger JM, Allen PB, Greengard P, Muallem S (2005) Spinophilin regulates Ca2+ signalling by binding the N-terminal domain of RGS2 and the third intracellular loop of G-protein-coupled receptors. *Nat Cell Biol* **7:** 405–411

Whorton MR, Bokoch MP, Rasmussen SG, Huang B, Zare RN, Kobilka B, Sunahara RK (2007) A monomeric G protein-coupled receptor isolated in a high-density lipoprotein particle efficiently activates its G protein. *Proc Natl Acad Sci USA* **104:** 7682–7687

Witt-Enderby PA, Jarzynka MJ, Krawitt BJ, Melan MA (2004) Knock-down of RGS4 and beta tubulin in CHO cells expressing the human MT1 melatonin receptor prevents melatonin-induced receptor desensitization. *Life Sci* **75:** 2703–2715

Xie GX, Palmer PP (2007) How regulators of G protein signaling achieve selective regulation. *J Mol Biol* **366:** 349–365

Xu X, Zeng W, Popov S, Berman DM, Davignon I, Yu K, Yowe D, Offermanns S, Muallem S, Wilkie TM (1999) RGS proteins determine signaling specificity of Gq-coupled receptors. *J Biol Chem* **274:** 3549–3556

Zeng W, Xu X, Popov S, Mukhopadhyay S, Chidiac P, Swistok J, Danho W, Yagaloff KA, Fisher SL, Ross EM, Muallem S, Wilkie TM (1998) The N-terminal domain of RGS4 confers receptor-selective inhibition of G protein signaling. *J Biol Chem* **273:** 34687–34690